Electronic Supplementary Information

Tungsten Oxide Nanocrystals Doped with Interstitial Methylammonium Cations

Owen Kendall,[a] Lesly Viviana Melendez,[a] Merve Nur Guven Bicer,[a] Michael Wilms,[a] Joel Van Embden,[a] Daniel Gómez,[a] Arrigo Calzolari,[b] Deborah Prezzi,[,b] and Enrico Della Gaspera,[*,a]*

[1] School of Science, RMIT University, Melbourne VIC 3000, Australia

[2] CNR-NANO Istituto Nanoscienze, Centro S3, I-41125 Modena, Italy

Corresponding author: *enrico.dellagaspera@rmit.edu.au, deborah.prezzi@nano.cnr.it

Experimental methods

Materials:

Ammonium metatungstate (AMT, 99.99%), caesium acetate (99.99%), oleylamine (OLA, 70%), tetrachloroethylene (TCE, 99.5%), trifluoroacetic acid (99%) and rubidium iodide (99.9%) were purchased from Sigma Aldrich. Methylammonium iodide (>99.99%) and formamidinium iodide (>99.99%) were purchased from Greatcell solar materials. Toluene (99.95%), ethanol (99.95%) and methanol (99.98%) were purchased from Univar. All chemicals were used without further purification.

Nanocrystal synthesis:

The synthesis was adapted from existing protocols available for WO_3 NCs with some modifications. 0.1 mmol of AMT and 0-0.825 mmol MAI were placed in a 50 mL round bottom flask (RBF), to which 20 mL of oleylamine was added. This RBF was then connected to a standard Schlenk setup, heated to 80 °C under vacuum and degassed for 30 min. After degassing was complete, the reaction flask was then backfilled with nitrogen and heated to 250 °C (ramp rate ~10 °C/min) and held at this temperature for 2 hours. Upon completion of the reaction, the mixture was allowed to cool naturally, and the NCs were precipitated using ethanol, centrifuged at 3000 rcf for 20 min and then redispersed in toluene. This process was repeated two more times, with the particles being either stored in toluene (or tetrachloroethylene, TCE, for optical absorption spectroscopy) or dried into a powder. Samples with different dopants were prepared by replacing MAI with the desired amount of alkali metal or formamidinium precursors, and keeping all other reaction parameters constant.

Characterisation techniques:

X-ray diffraction (XRD) was conducted on powder samples using a Bruker D4 Endeavor diffractometer equipped with a Cu-Kα x-ray source (40 kV, 35 mA). Transmission electron microscopy (TEM) images were captured using a JEOL JEM-2100F microscope operating at 200 kV and equipped with a Gatan OneView camera. Samples for TEM were prepared by depositing NCs dispersed in toluene onto a carbon coated copper grid (ProSciTech) and dried under vacuum for several hours. Optical absorption spectroscopy of NC suspensions in TCE was conducted using an Agilent Cary 5000 UV-Vis-NIR spectrophotometer, and the spectra have been normalized in intensity at the plasmon peak. X-ray photoelectron spectroscopy (XPS) was carried out using a Kratos Axis Supra XPS equipped with a monochromated Al Kα X-ray source (E_{photon}= 1486.7eV) and a concentric hemispheric electron analyser.

Theoretical calculations:

Theoretical investigation of WO_3 doped with MA molecules was carried out by using a first-principles plane-wave pseudopotential implementation of density functional theory (DFT), as available in the Quantum ESPRESSO (QE) package.[1,2] The Perdew–Burke–Ernzerhof (PBE) generalized gradient approximation for the exchange-correlation functional was used,[3] together with Hubbard-like corrections on each chemical species for a better description of electronic properties. The optimized U values, resulting from a pseudohybrid Hubbard Density Functional approach,[4] hereafter called U-ACBN0, are: U3d(W) = 0.174605 (0.174707) eV, and U2p(O) =

8.506185 (8.460920) eV for cubic (hexagonal) WO_3. This approach leads to improved band gaps with respect to the usage of the standard U3d(W) = 6 eV (see values in parentheses) for the undoped systems: E_g(c-WO_3) = 1.81 (1.07) eV; E_g(h-WO_3) = 1.84 (1.12) eV, in the range of those reported using hybrid functionals.[5] Lattice parameters are also mostly improved, as reported in the table below for undoped and doped WO_3, as well as undoped $W_{18}O_{49}$ (cod-id: 1001678). Lattice parameter values are in Å, angles in degree.

System	U=6	U-ACBN0	Experimental	Ref.
c-WO_3	3.8243	3.7985	3.74,3.77	6,5
h-WO_3 (a)	7.4380	7.3997	7.298	6
(c)	3.8243	3.7986	3.899	
$W_{18}O_{49}$ (a)		14.0834	14.028	7
(b)		18.4022	18.318	
(c)		3.7878	3.7828	
α, β, γ		90, 90, 115.088	90, 90, 115.211	
Cs @ h-WO_3 (a)	7.4754	7.4372	7.38	6
(c)	3.8466	3.8189	3.785	

Dispersion corrections were included in an optimized vdW-DF-like scheme for the optimization of doped WO_3.[8] Norm-conserving pseudopotentials were employed as available in the PseudoDojo Library.[9] The kinetic energy cutoff for the Kohn–Sham wave functions was set to 100 Ry, and the Brillouin zone was sampled with a uniform k-points density of 0.1 $Å^{-1}$, where the grid was generated according to the Monkhorst-Pack scheme. The optimized lattice parameters were obtained through a variable-cell optimization method, as implemented in QE. The atomic positions within the cell were fully relaxed until forces were less than 0.01 meV/Å, while cell pressure was kept lower than 0.1 Kbar. Ball-and-stick models of h-WO_3 and pseudocubic $W_{18}O_{49}$, including the identification of the unit cells are reported in Figure S1.

Estimation of carrier density from LSPR frequency:

The LSPR frequency ω_r depends on both the electron density and aspect ratio of the nanoparticles. From the electrostatic eigenmode method,[10] we know that:

$$\epsilon_M(\omega_r) = \epsilon_b \frac{1+\gamma}{1-\gamma}$$

where γ is a dimensionless quantity that depends on the particle geometry (more specifically, it is the eigenvalue of the so-called electrostatic eigenvalue equation), ϵ_b is the dielectric constant of the medium surrounding the nanoparticles (2.4 for TCE) and ϵ_M is the real part of the permittivity of a Drude metal:

$$\epsilon_M(\omega) = 1 - \left(\frac{\omega_P}{\omega}\right)^2$$

where:

$$\omega_P^2 = N\frac{e^2}{\epsilon_0 m}$$

is the plasma frequency, that depends on the electron density N of the material (here e is the electron charge, ϵ_0 is the permittivity of free space and m is the electron mass).

This means that it is possible to estimate N with knowledge of ω_r (from optical absorption measurements) and γ for each particle geometry according to:[10]

$$N = \left(\frac{1}{\epsilon_b} - \frac{1+\gamma}{1-\gamma}\right)\frac{\epsilon_b \epsilon_0 m}{e^2}\omega_r^2$$

Figure S1

Ball-and-stick models of h-WO_3 (left) and pseudocubic $W_{18}O_{49}$ (right). The unit cell used for the calculations is indicated with grey lines and replicated for clarity. W (O) is depicted in grey (red); the insets show the size of the void filled with MA molecules in the two cases.

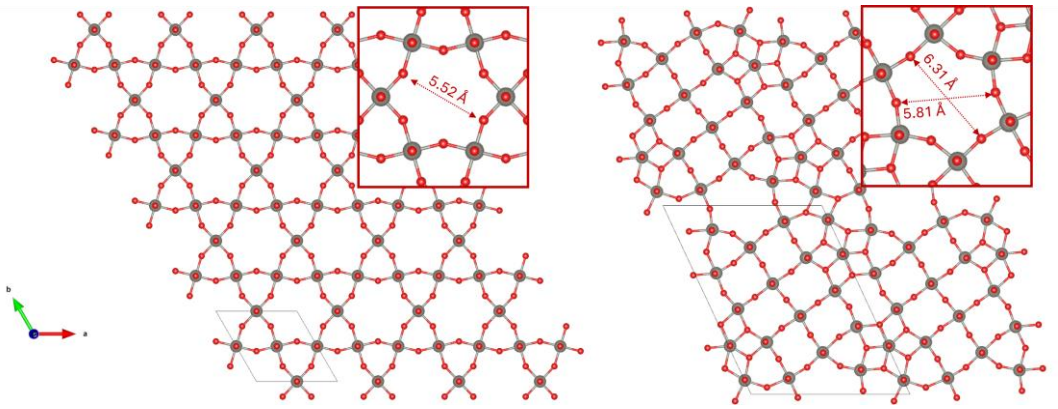

Figure S2

XRD patterns of WO_{3-x} NCs synthesised using various amounts of the MAI dopant as indicated on the side. Expected peak positions for cubic tungsten oxide (black lines, ICDD: 41-0905) and monoclinic oxygen deficient tungsten oxide (red lines, ICDD: 71-2450) are shown at the bottom.

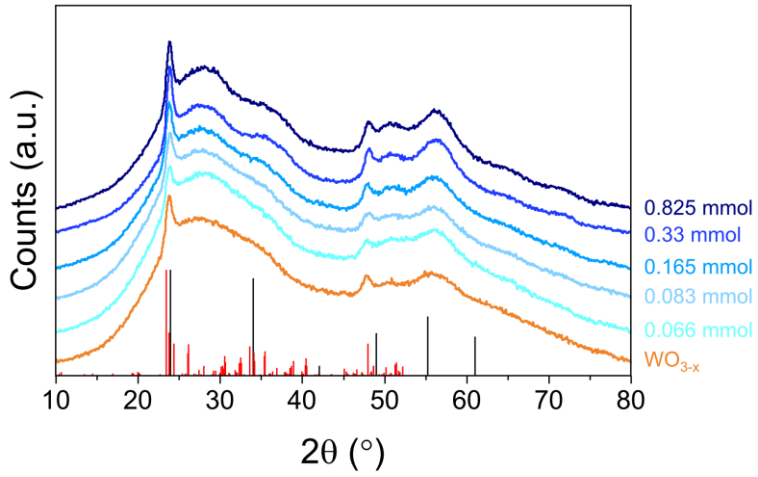

Figure S3

Comparison of XRD pattern of undoped WO_{3-x} NCs, and of WO_{3-x} NCs doped with methylammonium (MA) and rubidium (Rb). Expected peak positions for cubic WO_3 (black lines, ICDD: 41-0905) and monoclinic $WO_{2.72}$ (red lines, ICDD: 71-2450) are shown at the bottom.

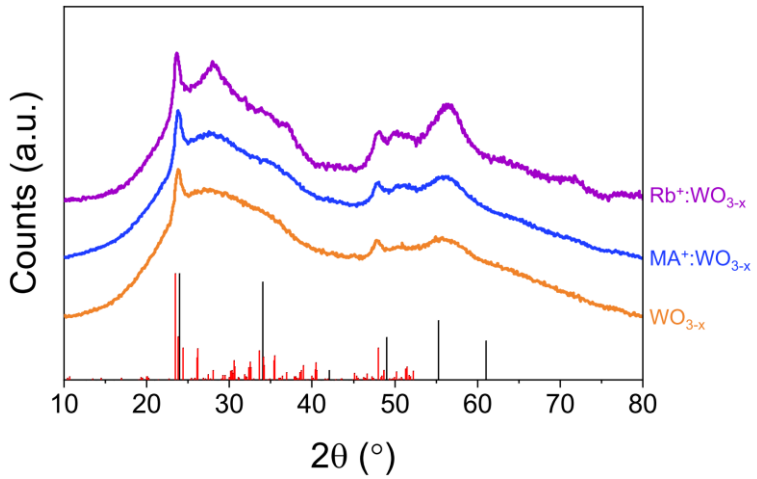

Figure S4

XRD patterns of WO_3 NCs doped with various amounts of caesium acetate as indicated on the side. A mixture of hexagonal $Cs_{0.32}WO_3$ (blue lines, ICDD: 83-1334) and cubic $(Cs_2O)_{0.44}W_2O_6$ (black lines, ICDD: 47-0566) is observed, with higher dopant loading promoting the formation of $(Cs_2O)_{0.44}W_2O_6$.

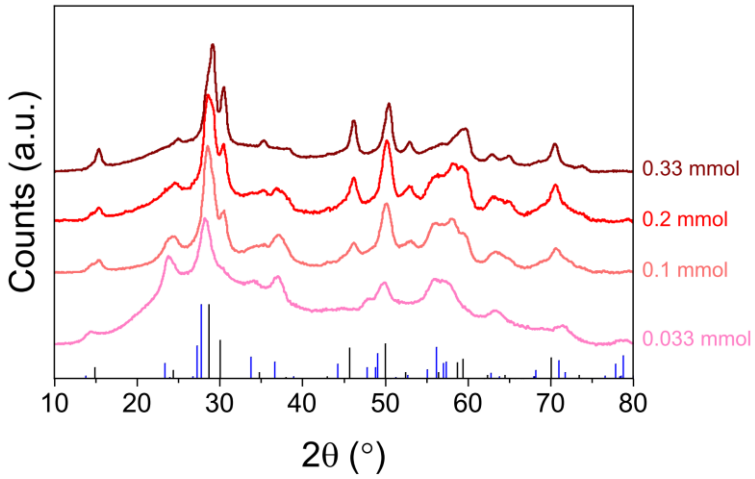

Figure S5

Additional TEM images of WO_{3-x} NCs (top row) and MA-doped WO_{3-x} NCs (bottom row).

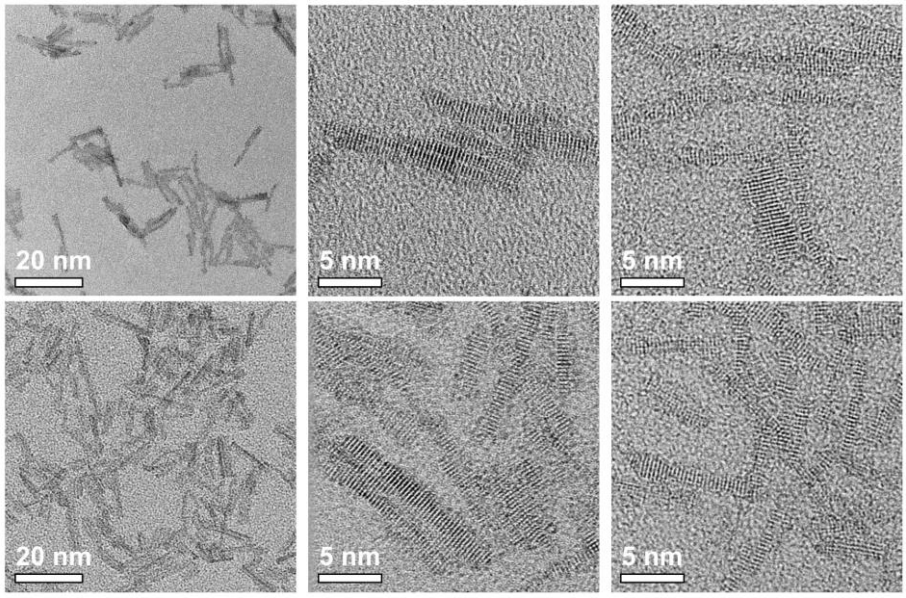

Figure S6

TEM images of WO_{3-x} nanocrystals synthesised using 0.33 mmol (left, aspect ratio ~7.2) and 0.825 mmol (right, aspect ratio ~7.5) MAI.

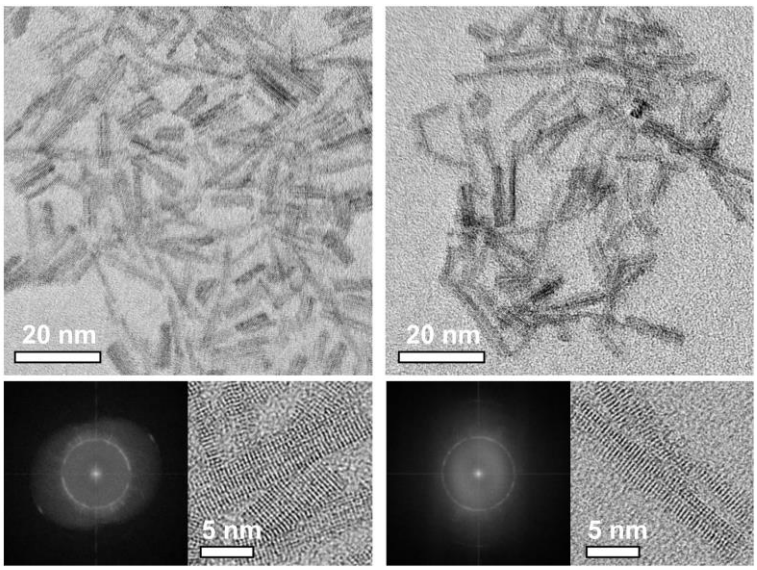

Figure S7

Typical XPS survey of MA^{+}:WO_{3-x} NCs.

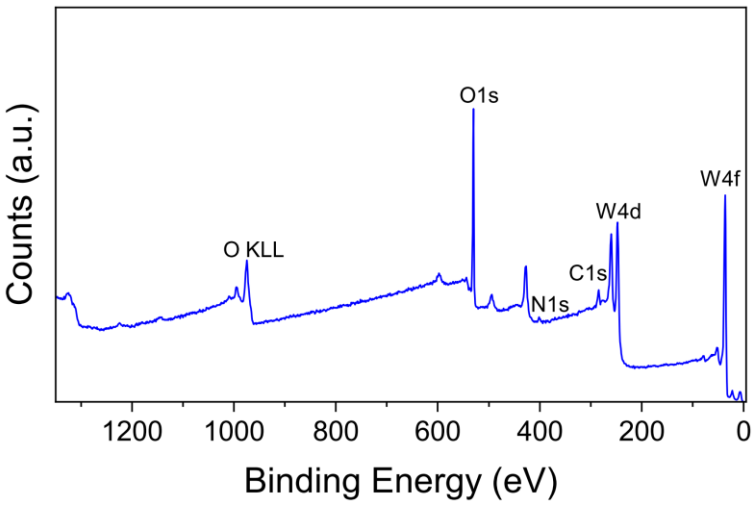

Figure S8

a) XPS of the O1s region of undoped WO_{3-x} and MA-doped WO_{3-x} NCs. b) Fitting of the O1s region for doped NCs.

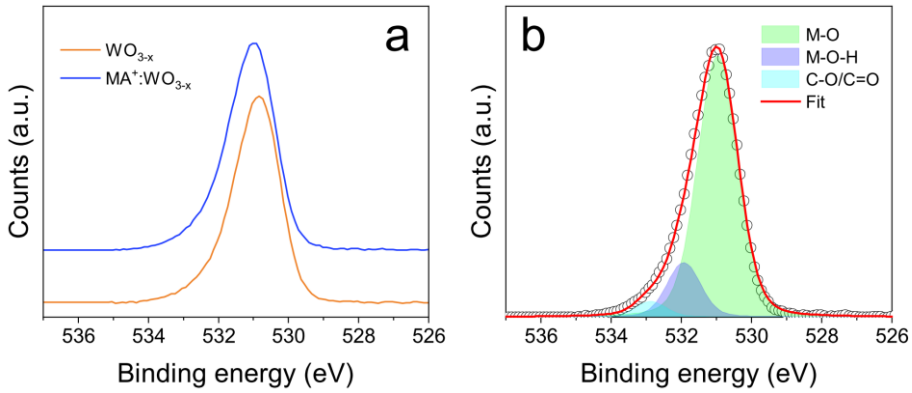

Figure S9

Plot of the W^{5+}: W^{6+} atomic ratio detected from XPS analysis as a function of the nominal amount of MAI used. The dashed line is just a guide to the eye.

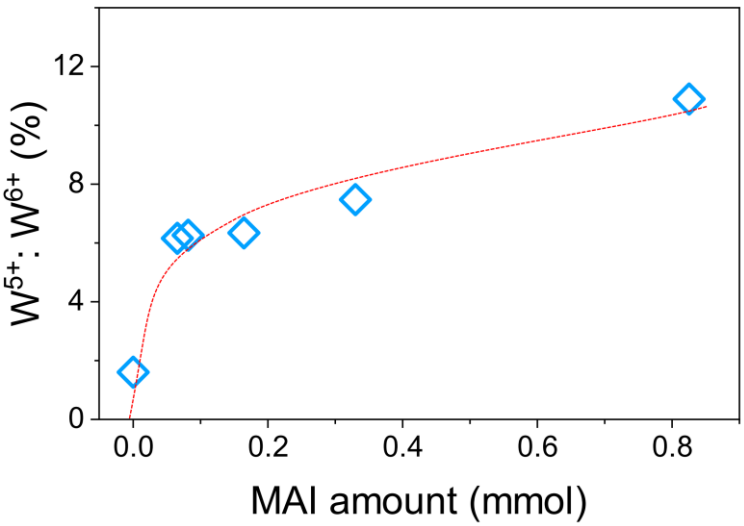

Figure S10

Density of states (DOS) for h-WO_3, both undoped (grey area) and doped with Cs (black curve) and MA molecules with different orientations with respect to the WO_3 framework, i.e., C—N axis parallel (blue curve) or perpendicular (orange curve) to the z axis. As can be seen from the relative position with respect to the Fermi level, the doping effect due to MA is the same than that induced by Cs atoms. Moreover, the molecule orientation does not impact significantly the electronic and doping properties of WO_3.

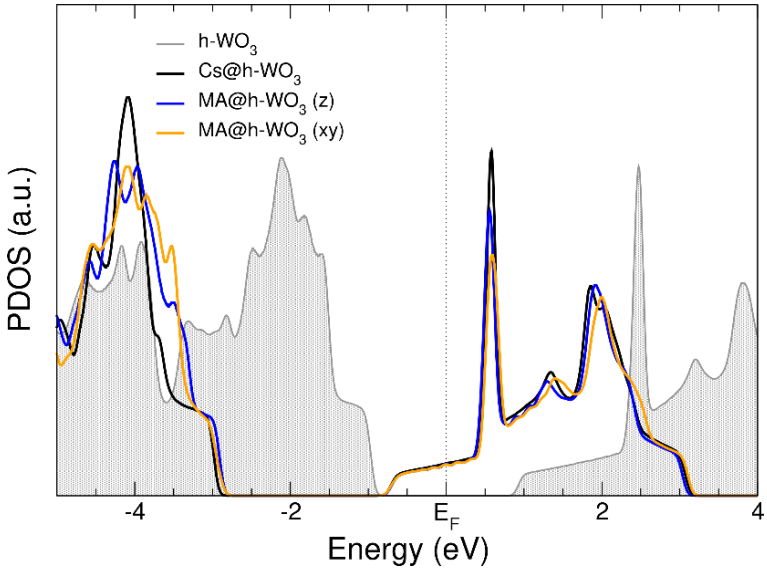

Figure S11

UV-vis-NIR spectra of equally concentrated solutions of WO_{3-x} NCs synthesised with and without MAI.

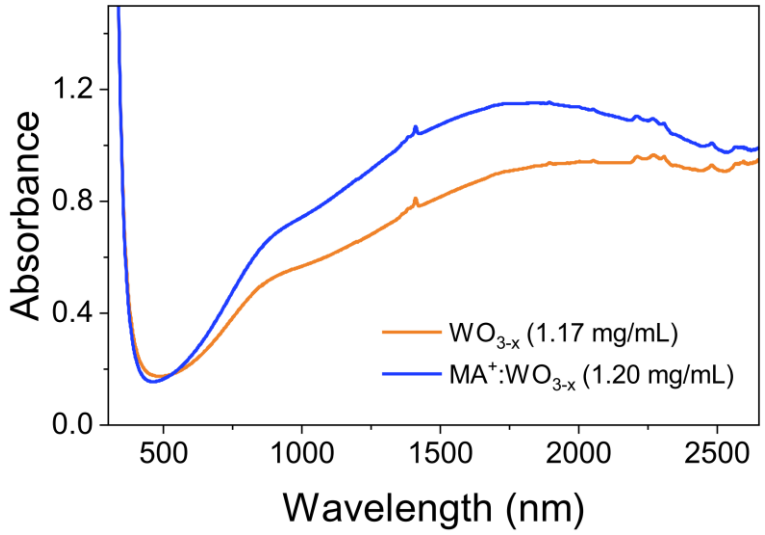

Figure S12

UV-vis-NIR spectra of WO_{3-x} NCs synthesised with different amounts of MAI. The spectra have been normalized in intensity at the LSPR maximum.

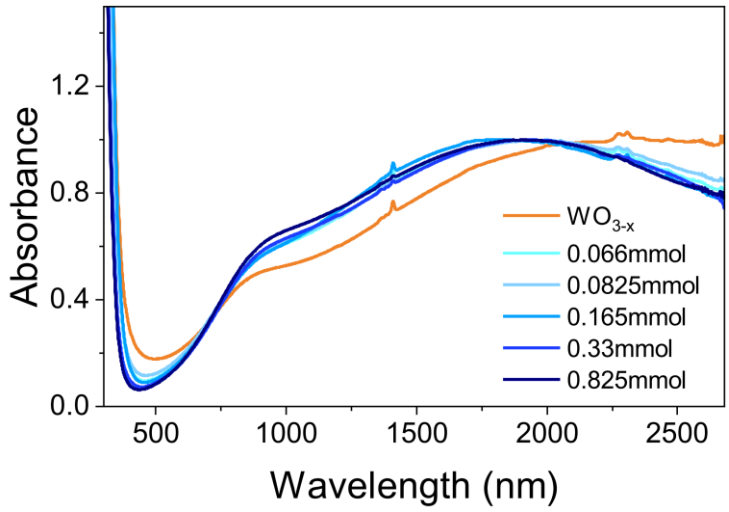

Figure S13

XRD patterns of tungsten oxide NCs doped with varying amounts of formamidinium (FA). Expected peak positions for cubic WO_3 (black lines, ICDD: 41-0905) and monoclinic $WO_{2.72}$ (red lines, ICDD: 71-2450) are shown at the bottom.

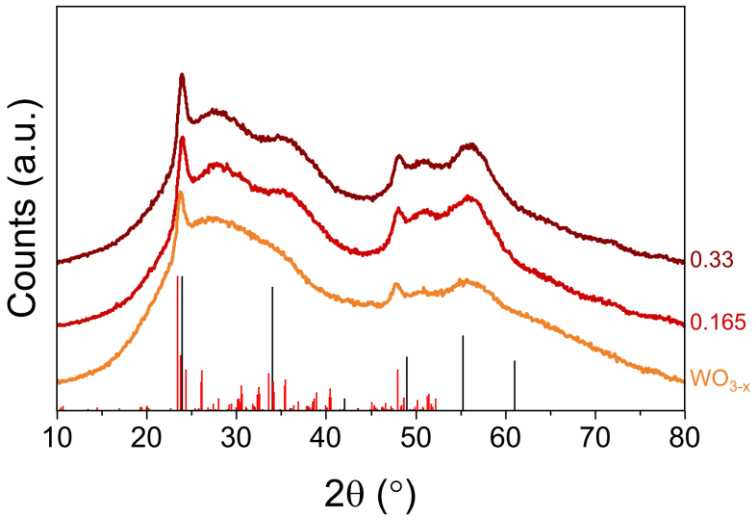

Table S1
W^{5+}:W^{6+} ratio in tungsten oxide doped with various amounts of MAI.

MAI (mmol)	W^{5+} at%	W^{6+} at%	W^{5+}: W^{6+} (%)
0 (undoped)	1.6	98.4	1.6
0.066	5.8	94.2	6.2
0.0825	5.9	94.1	6.3
0.165	5.9	94.1	6.3
0.33	7.0	93.0	7.5
0.825	9.8	90.2	10.9

Table S2
Comparison of peak area ratios of the two components N(I) and N(II) of the N1s XPS region for doped NCs before and after the treatment with TFA.

	N(I) (%)	N(II) (%)	N(I):N(II)
Pre-TFA	62.7	37.3	1.7
Post-TFA	87.2	12.8	6.8

Supporting References

(1) Giannozzi, P.; Baroni, S.; Bonini, N.; Calandra, M.; Car, R.; Cavazzoni, C.; Ceresoli, D.; Chiarotti, G. L.; Cococcioni, M.; Dabo, I.; et al. QUANTUM ESPRESSO: a modular and open-source software project for quantum simulations of materials. *Journal of Physics: Condensed Matter* **2009**, *21* (39), 395502. DOI: 10.1088/0953-8984/21/39/395502.
(2) Giannozzi, P.; Andreussi, O.; Brumme, T.; Bunau, O.; Buongiorno Nardelli, M.; Calandra, M.; Car, R.; Cavazzoni, C.; Ceresoli, D.; Cococcioni, M.; et al. Advanced capabilities for materials modelling with Quantum ESPRESSO. *Journal of Physics: Condensed Matter* **2017**, *29* (46), 465901. DOI: 10.1088/1361-648X/aa8f79.
(3) Perdew, J. P.; Burke, K.; Ernzerhof, M. Generalized Gradient Approximation Made Simple. *Physical Review Letters* **1996**, *77* (18), 3865-3868. DOI: 10.1103/PhysRevLett.77.3865.
(4) Agapito, L. A.; Curtarolo, S.; Buongiorno Nardelli, M. Reformulation of $\mathrm{DFT}+U$ as a Pseudohybrid Hubbard Density Functional for Accelerated Materials Discovery. *Physical Review X* **2015**, *5* (1), 011006. DOI: 10.1103/PhysRevX.5.011006.

(5) Wang, F.; Di Valentin, C.; Pacchioni, G. Electronic and Structural Properties of WO3: A Systematic Hybrid DFT Study. *The Journal of Physical Chemistry C* **2011**, *115* (16), 8345-8353. DOI: 10.1021/jp201057m.
(6) Ingham, B.; Hendy, S. C.; Chong, S. V.; Tallon, J. L. Density-functional studies of tungsten trioxide, tungsten bronzes, and related systems. *Physical Review B* **2005**, *72* (7), 075109. DOI: 10.1103/PhysRevB.72.075109.
(7) Lamire, M.; Labbe, P.; Goreaud, M.; Raveau, B. Refinement et nouvelle analyse de la structure de W18O49. *Revue de Chimie Minerale* **1987**, *24*, 369-381.
(8) Klimeš, J.; Bowler, D. R.; Michaelides, A. Van der Waals density functionals applied to solids. *Physical Review B* **2011**, *83* (19), 195131. DOI: 10.1103/PhysRevB.83.195131.
(9) van Setten, M. J.; Giantomassi, M.; Bousquet, E.; Verstraete, M. J.; Hamann, D. R.; Gonze, X.; Rignanese, G. M. The PseudoDojo: Training and grading a 85 element optimized norm-conserving pseudopotential table. *Computer Physics Communications* **2018**, *226*, 39-54.
(10) Davis, T. J.; Gómez, D. E. Colloquium: An algebraic model of localized surface plasmons and their interactions. *Reviews of Modern Physics* **2017**, *89* (1), 011003. DOI: 10.1103/RevModPhys.89.011003.